agronomy

MDPI

Article

Classification of the Nutritional Status of Peach Trees Using Indexes from Hyperspectral Images

Lourdes Lleó [1,*], Pilar Barreiro [1], Victoria Lafuente [2], Natalia Hernández-Sánchez [1] and Jesús Val [2]

[1] LPF_TAGRALIA—Técnicas Avanzadas en Agroalimentación, ETSIAAB, Universidad Politécnica de Madrid, CEI Moncloa, 28040 Madrid, Spain; pilar.barreiro@upm.es (P.B.); n.hernandez@upm.es (N.H.-S.)
[2] Departamento de Nutrición Vegetal, Estación Experimental Aula Dei (CSIC), Apartado 727, 50080 Zaragoza, Spain; mvlafuente@eead.csic.es (V.L.); jesus.val@csic.es (J.V.)
* Correspondence: lourdes.lleo@upm.es

Abstract: This paper presents a procedure for the comparison of two technologies developed to classify peach trees according to their nutritional status. The first technology uses the leaf SPAD-502 meter value to characterize tree classes as indicated by agronomist experts: sound, intermediate, and strong chlorosis trees. It is used as a reference for the second technology, which uses a combination of two multispectral indexes computed from reflectance hyperspectral images. Specifically, R_NDVI = (R800 − R670)/(R800 + R670) and HyperSPAD = (R940/R650) are computed for each leaf pixel. An automated methodology is proposed that sets two optical thresholds (three hyperspectral categories) in view of the outliers according to a normal distribution, together with an iterative optimization of the bounding that determines the best assignment of trees to one of the three SPAD_502 levels of nutritional status, as required for practical agronomical purposes such as fertilization. The Chi 2 distribution is used to confirm the similarity of both nutritional classifications. These results encourage the use of on-board multispectral cameras to monitor the nutritional status of trees and to establish a more efficient fertilization strategy where inputs are applied according to individual status, with the consequent reduction in losses of fertilizers such as nitrogen to the atmosphere, soil, and water resulting from over-application.

Keywords: precision agriculture; site-specific fertilization; optical properties; chlorosis; non-destructive on-board measurements

Citation: Lleó, L.; Barreiro, P.; Lafuente, V.; Hernández-Sánchez, N.; Val, J. Classification of the Nutritional Status of Peach Trees Using Indexes from Hyperspectral Images. *Agronomy* **2023**, *13*, 2713. https://doi.org/10.3390/agronomy13112713

Academic Editors: María Alonso-Ayuso, Guillermo Guardia and Zhaohai Bai

Received: 12 September 2023
Revised: 10 October 2023
Accepted: 25 October 2023
Published: 27 October 2023

1. Introduction

Peach (*Prunus persica* (L.) Batsch) is the most important temperate fruit tree grown in Spain, with 47.7 thousand hectares grown in 2019 and an equivalent production worth over EUR 380 million, according to the latest statistical data from the Spanish Agricultural Ministry (MAPA). The nutritional status of peach trees can be addressed based on the mineral analysis of either leaves or flowers [1–4]. The analysis of flowers anticipates the development of leaf chlorosis [4,5], though up to date it has not been possible to develop infield measurements of the mineral composition of flowers, whereas leaf chlorosis is well adapted to spectral measurements.

The optical properties of leaves depend on multiple biochemical and biophysical interactions. Interactions within the visible range (wavelength from 400 to 700 nm, VIS) are mainly influenced by leaf pigment content [6], such as the photosynthetic pigments chlorophylls, the photosynthetic accessory pigments carotenoids, and the non-photosynthetic pigments anthocyanins. In the near infrared range (wavelength from 700 to 1100 nm, NIR), the light is internally scattered, as only water molecules produce absorption. The scattering processes within the leaf are a consequence of the internal cellular structure, especially at the interfaces of the cell membrane and air, where light can be reflected and refracted [6]. Therefore, the optical properties of leaves can provide information on

metabolism, disorders, and diseases potentially useful for the agronomic management of crops.

In a review paper, the nutritional status of fruits and vegetables was compared to the VIS-NIR spectral response, and the authors found that the absorbance at different wavelengths was related to chlorophyll, pigments, nutrients, water, and the chemical and physical state of the plants [7]. Healthy plants reflect little light in the VIS region, related to high pigment content, while reflectance in the NIR region is high, related to well-structured tissue.

For nutritional disorders such as ferric chlorosis in peaches, both ranges (VIS and NIR) are of great interest. The well-known symptom of leaves turning yellow appears as the production of chlorophyll decreases. In addition, the photosynthesizing processes are hindered, which involves leaf structural changes such as weight reduction in the abaxial cuticle, enlargement of the epidermal cells, reduction in the guard cell size, and mesophyll being more compacted and less porous [8].

A common and very simple approach is to use the optical properties of leaves, which are characterized by a combination of wavelengths for each spectral range (VIS and NIR). Such is the case of the soil-plant analysis development index (SPAD, Equation (1)) that is lineal proportional to (denoted by α) the ratio between transmittance at 940 nm (related to the thickness of the leaf and to water content) and transmittance at 650 nm (related to chlorophyll activity). The widespread SPAD_502 chlorophyll meter computes a spectral index at an area of 2 × 3 mm on the leaf. SPAD-502 values measured by transmittance have demonstrated an estimation ability of 99.6% of the chlorophyll content measured as a unit of leaf area (nmol/cm^2) [9]. In addition, SPAD_502 proved to be an interesting tool to estimate leaf tissue nitrogen in trees such as Macadamia. A positive monotonic relationship was found between SPAD values and nitrogen [10]. A disadvantage of using handheld SPAD chlorophyll meters is the limited number of measurements that can be carried out per leaf.

$$\text{SPAD } \alpha \ \log\frac{T_{940}}{T_{650}} = \log\frac{I_{940}/I_{0\ 940}}{I_{650}/I_{0\ 650}} = \log\frac{I_{0\ 650}\ I_{940}}{I_{650}\ I_{0\ 940}} \quad (1)$$

Previous research with data gathered from three seasons [2,3] showed that the SPAD measured locally by transmission on leaves appeared to be correlated to the Ca and Sr content in flowers. Generally, the SPAD values above 32 corresponded to sound trees, while values below 24 points corresponded to intense leaf chlorosis (visible to the naked eye), with leaf nutrition levels below 60 mg kg^{-1} Fe and 1.6 g 100 g^{-1} Ca, measured by mass spectrometry. The relationship between SPAD values in the leaves and iron content (Fe) was also studied [2,3]. The authors observed a large decrease in both the SPAD and Fe ions in 2016 compared to 2014; Ca and Fe showed a significant relationship among them at leaf level.

Another approach that has been considered for the analysis of the nutritional status of peach trees is the use of a reflectance hyperspectral imaging system (HSI). Hyperspectral imaging has often been used to assess the nutritional status of vegetation. Different applications of HIS on plants cover foliar nutrition estimation, variety identification, growth monitoring, stress, and disease-related studies, among others [11].

A high number of spectra are acquired from the leaves with a high spatial resolution of 0.26 × 0.26 mm in this study, providing a series of detailed images for every wavelength comprising the spectral range.

By using HSI, dedicated spectral indexes can be computed and evaluated. Virtual images can be created with the selected spectral indexes computed for each pixel. Thus, a leaf is characterized by thousands of values spatially distributed throughout the entire surface. The growth condition and nutritional status of maize were monitored using SPAD estimated values as references [12]. Multi-spectral images were acquired from a UAV platform at different growth stages. SPAD values were estimated from both spectral and textural indices extracted from the images by using machine learning methods. Support vector machine (SVM) performed the best with 0.81 R^2 and 0.14 RMSE values.

In most cases, chlorosis starts on the youngest or apical leaves, located at the exterior of the canopy, affecting all branches in the same way. These characteristics may facilitate the inspection of the crop using on-board sensors based on multispectral indexes obtained from HSI. Therefore, such inspection can help in the diagnosis of deficient nutritional status in a non-destructive, non-contact, and faster way compared to manual SPAD measurements. The individual characterization of the nutritional status of each tree is the basis of an efficient fertilization strategy, which leads to the consequent reduction in losses of fertilizers, such as nitrogen, either to the atmosphere, soil, and/or water, generally derived from local overdose.

This work aims to develop a procedure to classify peach trees according to three classes of nutritional status by selecting proper thresholds for the frequency of multispectral indexes within the entire surface of the leaves. Classes of nutritional status are specified by agronomist experts and characterized by a global SPAD value from each leaf. Specifically, two multispectral indexes have been computed by combining the reflectance at different wavelengths: HyperSPAD as (R940/R650) and R_NDVI as [(R800 − 670)/(R800 + R670)], from now onwards R_NDVI. The HyperSPAD index will be compared to SPAD transmittance measurements since it considers the same wavelengths (however, in reflectance mode). On the other hand, the R_NDVI is considered a complementary parameter, being one of the standard remote references for assessing crops [13].

2. Materials and Methods

2.1. Experimental Plot

The trial was conducted in 2016 and 2017 in a plot located at the Aula Dei Experimental Station (Consejo Superior de Investigaciones Científicas, Zaragoza, Spain) (Longitude: 0°49′45″ W, Latitude: 41°43′15″ N, Altitude: 210 m), in charge of the experimental design, aimed at determining the sensitivity of different grafting rootstocks with respect to nutritional deficiencies in calcareous soil of large varying nature in Caterina peach trees. The soil of the plot is heavy and calcareous, with 30.5% calcium carbonate, 8.8 active silt, and a clay-loam texture. The pH of the water was 7.7. The rootstocks used were plum × peach: Adesoto 101, PM 105 AD, P. Soto 67, Constatí 1, Montizo, GF 655. The grafted variety was peach 'Catherina'.

Thirty-two peach trees were selected. For each tree, nine leaves were picked from the middle of bearing shoots located all around the crown from the outer part of the tree canopy 120 days after full bloom. Leaves were randomly selected per tree by experts as representative of different chlorosis stages; among the leaf samples, random resampling was carried out so as to split them out into three subsamples per tree, considering leaf variability as representative of tree heterogeneity. In the field, measurements were made with a SPAD_502 meter (Minolta Co., Osaka, Japan) on the first subsamples. Three SPAD values were obtained per leaf and nine values per tree, the total of SPAD measurements being n = 288. The other two groups of subsamples were transported in refrigerated containers. One subsample was used for the analysis of the mineral composition, including macro- and micronutrients, by means of plasma-mass spectrometry (subcontracted at CEBAS-CSIC, Murcia, Spain, http://www.iqog.csic.es/es/servicios-iqog/servicio-de-espectrometria-de-masas, accessed on 1 September 2023). Additionally, mineral composition was also estimated on flower samples (10 g per sample); flower sampling was carried out at full bloom in the middle of March [2,3].

The third subsample was used for the acquisition of hyperspectral images. They were transported in refrigerated and insulated boxes to the laboratory in Madrid. Measurements were taken on the same date as the harvest date. The HSI was composed of a Headwall Photonics camera, HyperspecTM VNIR (400 to 1000 nm), a halogen lamp, a pushbroom (for scanning purposes), and a sample presentation corresponding to 0/45 geometry (Headwall Photonics Hyperspec-VNIR™, Fitchburg, MA, USA). Hyperspectral images were acquired with a spatial resolution of 260 nm × 260 nm and a spectral resolution of 3.2 nm. Reflectance images were computed considering, for each pixel, the dark current (0 value) and the white

reference values (100% reflectance) obtained from a barium sulphate bar. The same number of reflectance spectra, n = 1460, was randomly selected for each leaf. Thus, the total number of spectra was 4380 per tree and 140,160 for the 32 trees under study.

2.2. Macro and Micronutrients at Flower and Leave Level and Their Relation with SPAD Measurements

Table 1 shows macronutrients (% of dry matter) at flower and leaf levels. Leaves show higher average values than flowers for K, Ca, and Mg while being lower for P and S. Leaves generally show greater CV than flowers, with the largest variability corresponding to Ca in both flowers (CV = 11.7%) and leaves (CV = 21.90%) [3].

Table 1. Macronutrients at flower and leaf level in percentage of dry matter (%).

		K	Ca	P	Mg	S	C	N
Flower	Average	1.83	0.48	0.38	0.18	0.14		
	STD	0.14	0.06	0.03	0.01	0.01		
	%CV	7.65	11.76	9.00	6.35	8.19		
Leaves	Average	2.57	1.42	0.17	0.33	0.12	42.32	2.88
	STD	0.29	0.31	0.02	0.04	0.01	0.68	0.25
	%CV	11.14	21.90	13.00	11.42	10.16	1.61	8.56

Table 2 shows the eight most relevant micronutrients. The amount of micronutrients in the flowers is higher than that of leaves (leave to flower ratio below 1) for Na, Al, Fe, and Cu, while being lower for Sr, Mn, and B. A very large difference in average value is found for Cu, Na, and Fe between flowers and leaves: 77.1 vs. 7.38 mg/kg for Cu, 176.9 vs. 46 mg/kg for Na, and 146.7 vs. 71.60 mg/kg for Fe. The highest variability in micronutrients for leaves also corresponds to Na, Al, and Fe (CV = 31.8%, 24.4%, and 18.9%) compared to flowers (CV = 19.7%, 19.1%, and 13.8%).

Table 2. Micronutrient (mg kg^{-1}) at flower and leaf level.

		Na	Al	Fe	Cu	Zn	Sr	Mn	B
Flower	Average	176.9	152.4	146.7	77.7	45.8	34.9	28.0	19.0
	STD	34.8	29.1	20.2	15.8	4.9	4.5	2.9	3.1
	%CV	19.7	19.1	13.8	20.3	10.6	13.0	10.2	16.4
Leaves	Average	46.0	71.60	46.39	7.38	24.63	149.91	40.71	26.35
	STD	14.6	17.35	8.76	0.99	4.67	30.73	5.23	3.45
	%CV	31.8	24.24	18.89	13.47	18.98	20.50	12.85	13.11

Table 3 shows the linear correlation coefficients between macro elements and SPAD at the flower and leaf levels. The correlation coefficients between macronutrients and SPAD are significant at leaf level for K, Ca, and S, while at the flower level only Ca seems related to SPAD [3].

Table 3. Linear correlation coefficients between macronutrients and SPAD at flower and leaf levels (* and **, 1 and 5 significance levels, respectively) [3].

	K	Ca	P	Mg	S
FLOWER	ns	0.4455 **	ns	ns	ns
LEAVE	−0.3091 **	0.4736 **	ns	−0.1487 *	0.4336 **

Table 4 shows the linear correlation coefficients between microelements and SPAD at the flower and leaf levels. As before, higher correlation coefficients are found at the leaf level as well as at the flower level. For leaves, Fe, Cu, Sr, and B seem relevant, while at flower level, only Sr shows a significant correlation [3].

Table 4. Linear correlation coefficients between micronutrients and SPAD at flower and leaf levels (* and **, 1 and 5 significance levels, respectively) [3].

	Na	Al	Fe	Cu	Zn	Sr	Mn	B
FLOWER	ns	−0.1517 *	0.1460 *	0.1854 *	ns	0.4096 **	0.1200 *	0.2099 *
LEAVE	ns	ns	0.3345 **	0.3092 **	0.1049 *	0.4565 **	0.1448 *	−0.3710 **

2.3. Data Analysis Procedure

The results of the mineral analysis were considered by experts who established the thresholds of the infield SPAD value to assign each tree to one of three levels of nutritional status: no nutritional deficiency, intermediate status, and severe deficiency status. These classes were named SPAD Class 1, SPAD Class 2, and SPAD Class 3, respectively.

The methodology for HSI image data analysis consisted of five steps: A, B, C, D, and E (Figure 1). At step A, each tree was characterized by a range of two multispectral index values, HyperSPAD and R_NDVI, computed from the corresponding hyperspectral images of its leaves. An analysis of the median and interquartile ranges was carried out. The outliers, according to a normal distribution, were used to establish the nutrition thresholds of the HyperSPAD and R_NDVI indexes useful to classify the pixels into HSI-based Class 1 (sound), Class 2 (intermediate), and Class 3 (chlorosis).

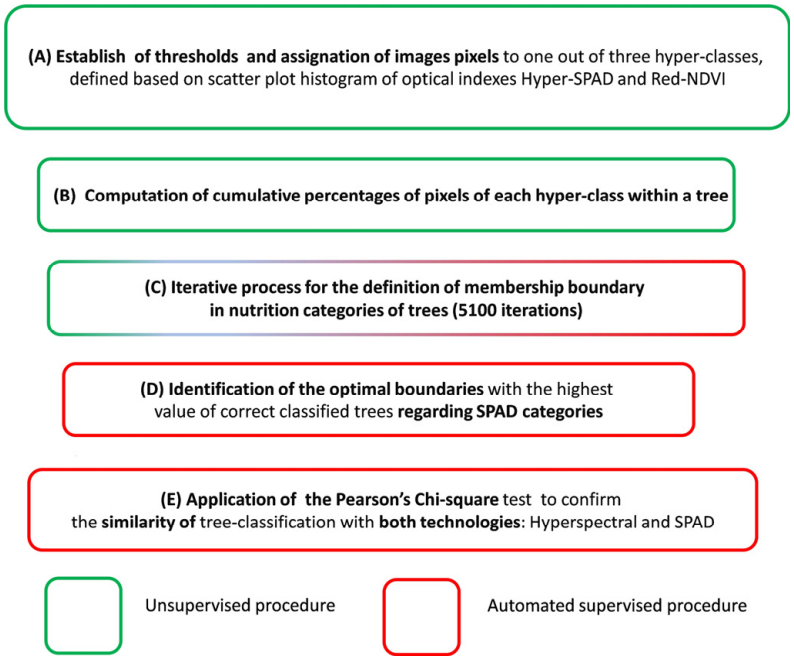

Figure 1. Summary of the proposed methodology for classifying the nutritional status of peaches using hyperspectral images.

Afterwards (step B), the cumulative percentage of the pixels per class was computed for each tree, and a bar plot was generated. Step C was established as an iterative procedure to generate three HSI-based tree categories (sound, intermediate, and chlorosis) that best fit the tree classification using the SPAD class as a reference. To this end, the boundaries of membership for each HSI-based class were optimized. The iterative process was defined with boundaries increasing from 0 to 100% of pixels belonging to HSI-based Class 1 (i-value) and of pixels belonging to hyper-Class 3 (j-value), with $i + j < 100\%$; 5100 iterations were generated ($n = 101^2/2$). For each tree, at each step, when the percentage of HSI-based Class 1 pixels was higher than the i-value, the tree was classified as HSI-based Class 1, when the percentage of HSI-based Class 3 pixels was higher than the j-value, the tree was classified as HSI-based Class 3, and when none of the previous conditions were met, the tree was classified as HSI-based Class 2.

Under step D, the confusion matrixes between the tree HSI-based classification classes and SPAD categories were computed for the 5100 iterations (i-value, j-value), searching for the highest percentage of well-classified trees (maximization of trace), and moreover, extreme errors were evaluated (false extreme positives and negatives). Finally, in step E, the Pearson's Chi-square test was applied to confirm the significance of the similarity of the tree classification with both technologies.

3. Results

3.1. SPAD Measurements

Trees were assigned to three classes according to the mineral content and SPAD values of the trees by agronomist experts (explained in lines 76–85) [2,3]. The nine SPAD values for every tree within each class are depicted in Figure 2 as box and whiskers plots, with interquartile and whole range intervals, respectively. Class 1 comprised sound trees with an SPAD median value (and most of the interquartile box) above 32 and always higher than 24, so that there was not a single leaf with chlorosis affection. Class 3 comprised trees severely affected by chlorosis, with the SPAD median (and most of the interquartile box) below 24. In addition, Class 3 showed a wide SPAD dispersion, which highlighted the heterogeneity in the development of chlorosis within the tree. Class 2 comprised trees with an intermediate chlorosis level and a SPAD median between 24 and 32.

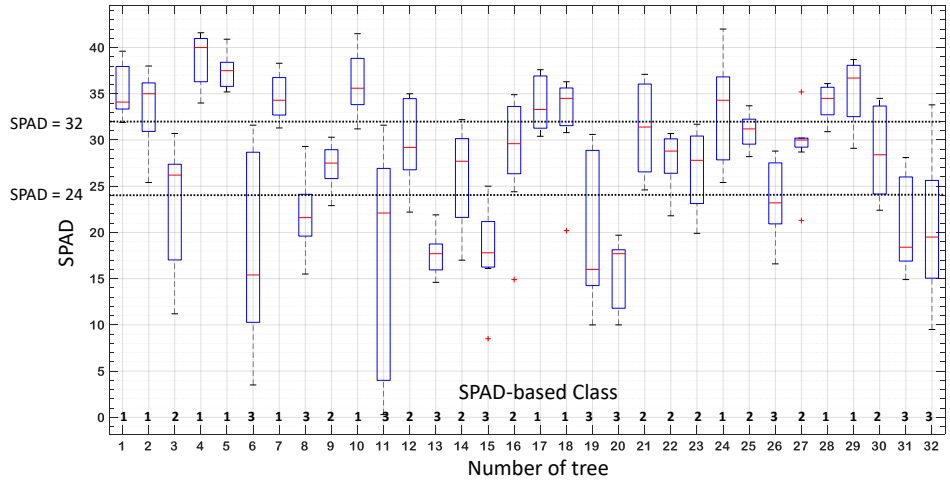

Figure 2. Ranges of SPAD values (n = 9 per tree) for each tree (1 to 32) as box and whiskers plots: median (horizontal red lines), interquartile, and whole range intervals; outliers are identified as red crosses. SPAD thresholds were highlighted, and nutrition classes were assigned (1 to 3) according to [2,3].

Ca and Sr were the most linearly correlated minerals with respect to SPAD (Tables 3 and 4). Figure 3 illustrates the positive relationship between those two mineral contents and the SPAD values.

3.2. Spectral Indexes from Hyperspectral Images

Multispectral indexes HyperSPAD and R_NDVI were computed from the HSI of the leaves, providing 4380 values for each index for each tree. Therefore, more detailed information was obtained, which potentially involved a more realistic characterization of the chlorosis development.

The use of data obtained from hyperspectral images allows for a shift from a leaf-level global categorization (healthy leaf, leaf with intermediate nutritional status, leaf with severe nutritional problems) provided by the SPAD meter to an intra-leaf categorization, as it is possible to identify within a leaf the proportion of pixels showing no nutritional deficiency symptoms (HSI-based Class 1), pixels with intermediate symptoms (HSI-based Class 2), and pixels with severe deficiency symptoms (HSI-based Class 3).

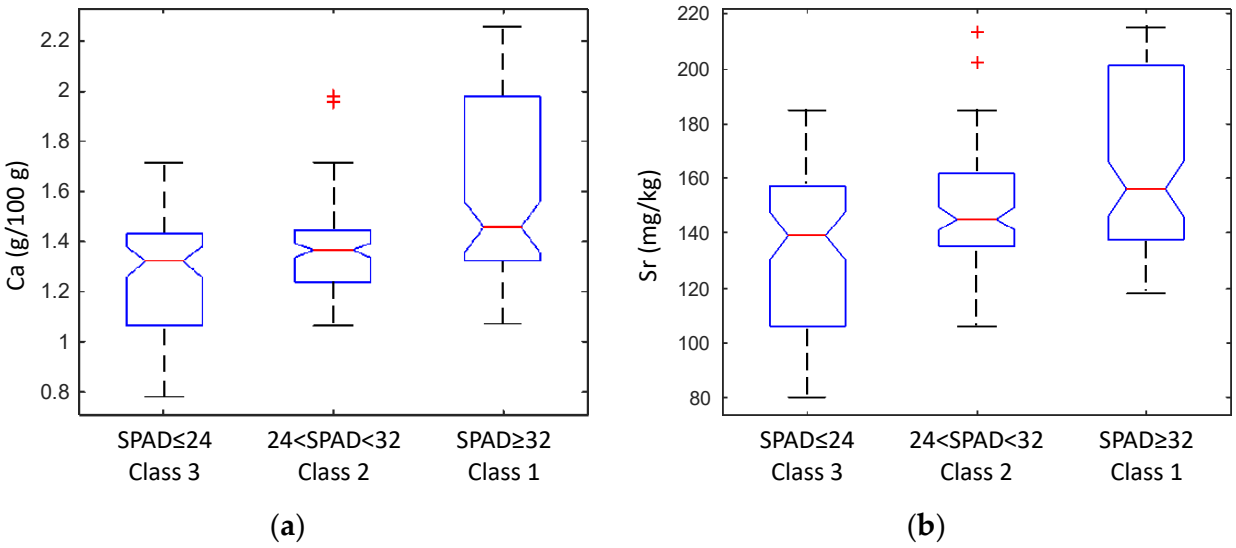

Figure 3. Mineral content of Ca (**a**) and Sr (**b**), considering the average SPAD values per tree and for each category of chlorosis as box and whiskers plots: median (horizontal red lines), interquartile, and whole range intervals; outliers are identified as red crosses.

The first step was to identify the thresholds of the HyperSPAD and R_NDVI indexes useful to classify the pixels into the corresponding HSI-based classes. Thresholds were established according to the scatter-histogram plot (Figure 3) and the range of index values as box and whiskers plots (Figure 4).

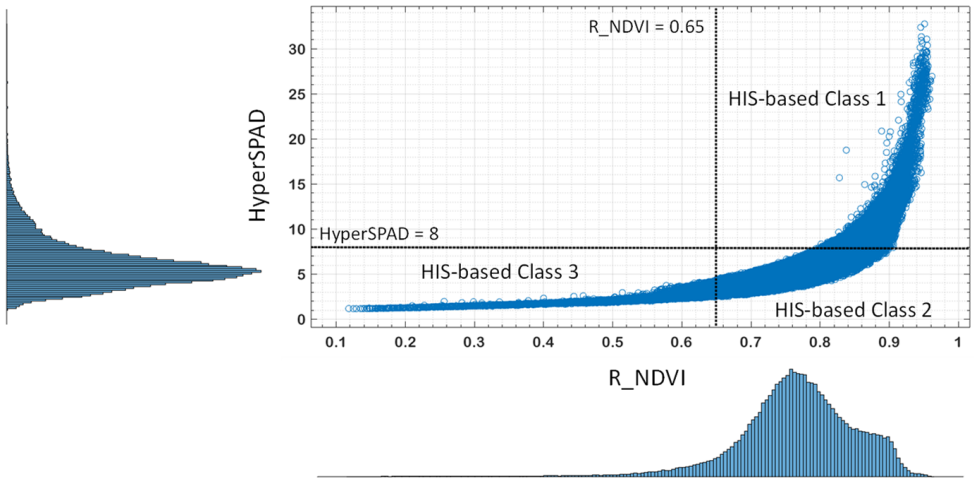

Figure 4. R_NDVI vs. HyperSPAD scatter-histogram plot. The vertical line at 0.65 of R_NDVI is considered to separate class 3 from class 2 pixels, whereas the horizontal line at 8 of HyperSPAD is considered a threshold between Class 1 and Class 3.

Figure 4 illustrates the distribution of the values of the multispectral indexes for the whole set of pixels (N = 140,160). The use of the R_NDVI index provided an additional criterion for the segregation of the pixels in this plot. For low HyperSPAD values, a high dispersion of the R_NDVI values is observed, whereas for high values of R_NDVI, a high dispersion of the HyperSPAD values is found.

Figure 5 shows the range of index values. Outliers are represented by red symbols (+). The large number of outliers was attributed to the huge number of values and the natural variability within the leaves. For the HyperSPAD index, most of the outliers presented a value higher than 8. This value was selected as the threshold for pixels with no chlorosis affection, HSI-based Class 1. As for the R_NDVI index, most of the outliers presented values lower than 0.65. This value was selected as the threshold for pixels of very chlorotic leaf tissues, HSI-based Class 3. Finally, HSI-based Class 2 comprised pixels with HyperSPAD below 8 and R_NDVI above 0.65. These thresholds are included in Figure 4 for graphical segregation of pixels.

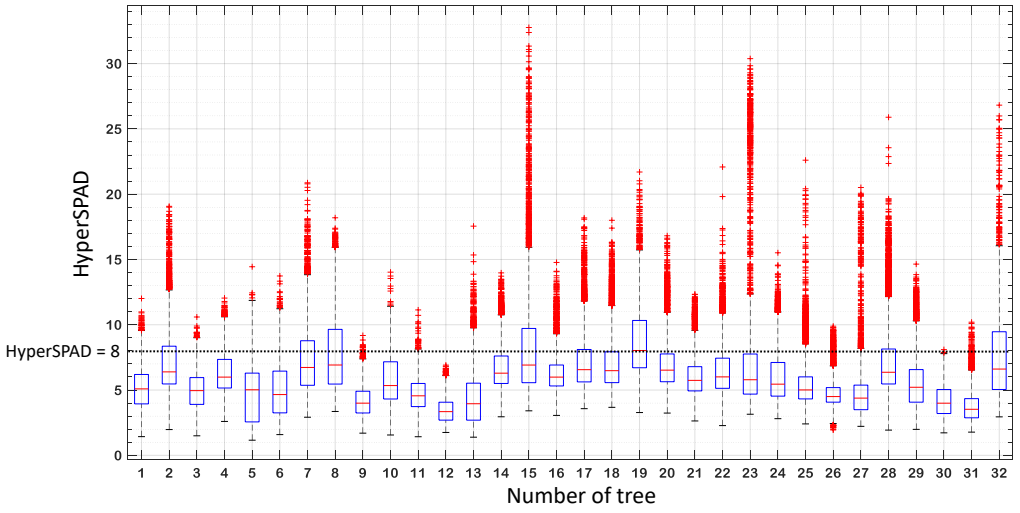

(**a**)

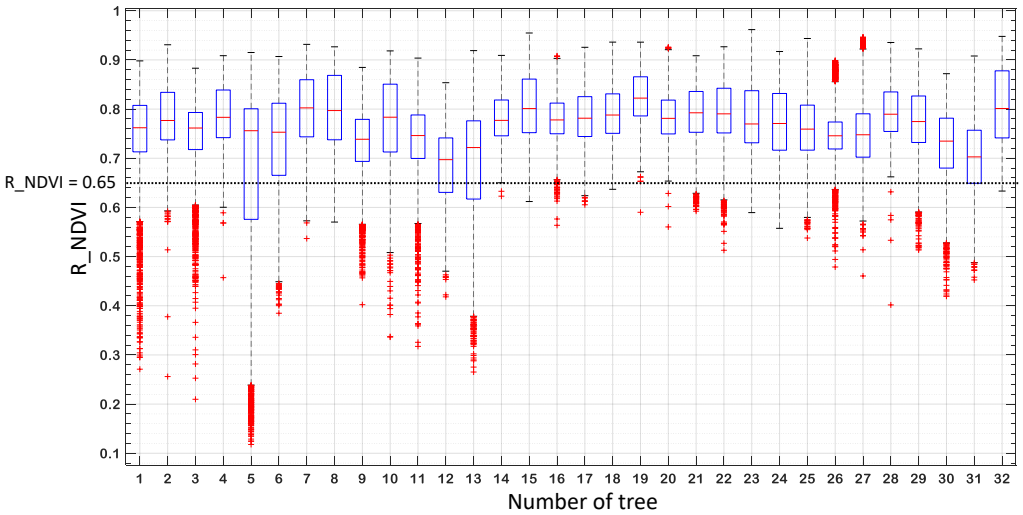

(**b**)

Figure 5. (**a**) HyperSPAD and (**b**) R_NDVI value ranges for each tree computed on hyperspectral images, 4380 data points per tree. Box and whiskers plots: median (horizontal red lines), interquartile, and whole range intervals; outliers are identified as red crosses.

3.3. Characterization of Trees Based on HSI Classification

Once the thresholds were set, the percentage of pixels was computed for each tree (Figure 6), which varied from one to another. Most trees presented pixels belonging to the three hyper-classes, while some trees presented pixels belonging to two classes (Classes 1 and 2 or 2 and 3).

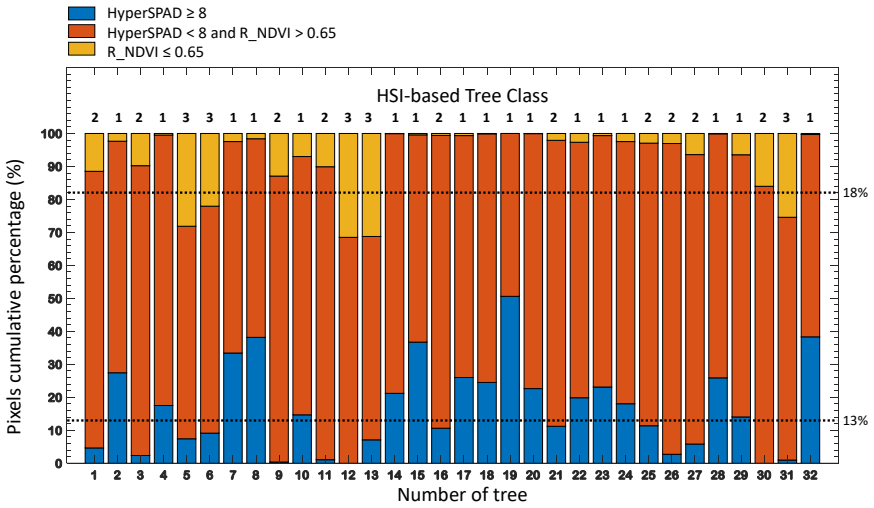

Figure 6. For each tree, vertical bars show the percentage of pixels using hyperspectral indexes (HyperSPAD and R_NDVI). Blue, red, and orange correspond to the percentage of pixels in Class 1, Class 2, and Class 3, respectively. Horizontal lines refer to thresholds for HSI-based tree classification.

3.4. Iterative Optimization Procedure

For practical agronomical purposes, each tree needs to be classified globally by assigning it to a single class. Then, the next step was to develop a procedure to establish the limits of the percentage of pixels belonging to each HSI-based class to provide a global tree classification (see Material and Methods, Section 2).

For each pair of percentage thresholds (percentage of HSI-based Class 1 pixels and Class 3 pixels), the confusion matrix was computed between the global HSI-based and the global SPAD classification. The trace of each matrix, i.e., the total number of trees whose classification matched, was calculated to evaluate the agreement between both classifications.

Figure 7 shows the value of all the traces in a color scale in a 2D plot with a percentage threshold of HSI-based Class 3 pixels in the X-axis and HSI-based Class 1 pixels in the Y-axis. For HSI-based Class 1, a percentage of 13% showed the best performance, as high trace values were obtained for all the HSI-based Class 3 thresholds.

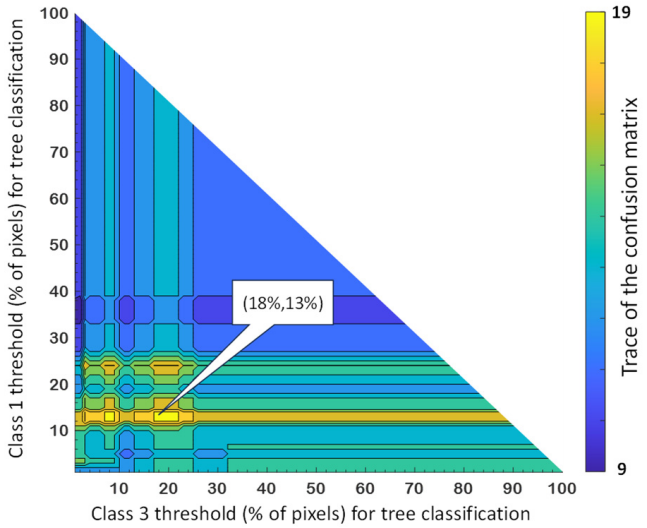

Figure 7. Trace of the confusion matrices for SPAD and HSI-based tree classification with variable pixel thresholds. Total of correctly classified trees in color scale for each pair of thresholds: 5100 instances.

The confusion matrix of one of the threshold pairs corresponding to the highest trace value (18%, 13%) is shown in Table 5. For this threshold pair, when the percentage of HSI-based Class 3 pixels was higher than 18%, the tree was classified as HSI-based Class 3, whenever the percentage of HSI-based Class 1 pixels was higher than 13%, the tree was classified as HSI-based Class 1, and if none of the previous conditions were met, the tree was classified as HSI-based Class 2.

Table 5. Confusion matrix with maximum coincidence between HSI and expert classification (SPAD_502 meter); thresholds: Class 1 pixels > 13%, and Class 3 pixels > 18%).

	SPAD_502			
HSI Based	**Class 1**	**Class 2**	**Class 3**	**Total**
class 1	9	3	5 [1]	17
class 2	1	7	2	10
class 3	1 [1]	1	3	5
Total	11	11	10	32

[1] Extreme errors.

The classifications matched for 19 out of 32 trees (59.4%). Classification errors were expected derived from some discrepancies found as a few trees (8, 15, 19, 20, 32) were characterized as trees severely affected by chlorosis using SPAD_502 meter classes while they did not show HSI-based Class 3 pixels.

The tree classification similarity between SPAD and multispectral indexes obtained from hyperspectral images was studied through a Pearson's Chi square test applied to the observed classification in comparison to what was expected (Table 6). Table 6 provides the figures corresponding to the observed and expected tree distribution among the three nutritional status classes. The Pearson's Chi square value calculated, χ^2 observed, was 3. The tabulated value, χ^2 tabulated, was 5.99, considering a 0.05 p-value and 2 degrees of freedom $[(2-1)\times(3-1)]$.

Table 6. Figures corresponding to observed (left) tree distribution among the three nutritional status classes and expected (right) when classification is not affected by the technology employed.

	Observed				**Expected**			
	Class 1	**Class 2**	**Class 3**	**Total**	**Class 1**	**Class 2**	**Class 3**	**Total**
SPAD_502	11	11	10	32	14	10.5	7.5	32
HIS	17	10	5	32	14	10.5	7.5	32
Total	28	21	15	64	28	21	15	64

4. Discussion

SPAD_502 meter and HSI strategies differ in their spectral modes, that is, transmittance and reflectance, respectively; hence, misclassification may arise from these differences. According to the bibliography, the reflectance spectra of the green parts in the leaves of C. blumei with different content of total chlorophyll presented a local maximum around 550 nm, with decreasing values towards the minimum around 680 nm [14]. However, for transmittance spectra, values from 550 to 650 nm were comparable, revealing that these wavelengths pass efficiently through the tissue and are better detected in transmittance mode. Behavior at wavelengths beyond 725 nm was also different, as reflectance spectra showed higher values than transmittance. Similar results were obtained for a range of chlorophyll levels in corn leaves established with N fertilizer applications [15]. Leaf transmittance was also found to be more sensitive to fertilization levels and chlorophyll content. The wavelength bands of light able to reach deeper into the leaf are more likely to interact with the light-absorbing molecules and with the tissue structure before leaving and being registered by the detector [16]. Such bands are effective sensors for molecule content and tissue integrity evaluation.

Despite that, encouraging results have been obtained with reflectance spectra. For peach tree, VIS-NIR reflectance spectra were used to classify leaves according to deficient (N < 2.99%), sufficient (N 3.00 to 3.50%), and excessive (N > 3.50%) nitrogen content [17]. Gaussian mixture discriminant analysis provided a spectral index combining values at 425 nm, 574 nm, 696 nm, and 700 nm that achieved a general correct classification rate of 75% under field conditions. Hyperspectral images were employed to predict potassium in peach leaves [18]. After applying the standard normal variate pre-treatment to the spectral region between 500 and 900 nm, the prediction model provided a coefficient of determination of 0.81 for validation data whose potassium content varied from 1.3 to 3.2%.

Resuming the classification errors in the present study (Table 5), only 18.7% appeared as extreme errors, that is, either they were classified as trees with poor nutritional status while being classified as sound trees by SPAD (4 out of 32), or they were classified as trees with good nutritional status while being classified as severely affected trees by SPAD (1 out of 32). Thus, 81.3% were acceptably classified according to their different levels of nutritional status, which would involve a more efficient use of the fertilizers compared to a blanket application where all the trees receive the same quantity of these inputs.

The similarity between the tree classifications using SPAD and multispectral indexes was confirmed by Pearson's Chi square test (Table 6). Pearson's Chi square value calculated (χ^2 observed = 3) was lower than the tabulated value (χ^2 tabulated = 5.99). Therefore, the number of trees classified within each class using either technology was similar. Thus, the total quantity of fertilizers applied according to either tree classification would be similar as well. Further work, including a higher number of trees and leaves per tree, as well as fertilization strategies, is recommended to validate the methodology presented.

5. Conclusions

Trees could be assigned to three classes according to their mineral nutrition status, and thresholds for infield SPAD values could be obtained with a commercial SPAD 502 meter (Minolta Co., Osaka, Japan) accordingly. The wide SPAD dispersion found for Class-3, severely affected, highlighted the heterogeneity in the development of chlorosis within the tree.

Multispectral indexes such as HyperSPAD and R_NDVI computed from hyperspectral images of the leaves provided a huge amount of data. This involved a detailed characterization of the whole leaf surface, additional criteria for the segregation of the pixels, and the establishment of HSI-based classes of nutritional status.

Pixels with a HyperSPAD value higher than 8 were considered to have no chlorosis affection. Pixels with an R_NDVI value lower than 0.65 were considered very chlorotic (HSI-based Class 3). HSI-based Class 2 comprised pixels with HyperSPAD below 8 and R_NDVI above 0.65.

The iterative procedure proposed for tree classification establishes the optimal thresholds for the percentage of pixels belonging to HSI-based Classes 1 and 3 (13% and 18%, respectively). For optimal thresholds, classification based on in-field SPAD values and classification based on HyperSPAD and R_NDVI values matched for 59.4% of the trees, with only 18.7% of extreme errors. Therefore, 81.3% of the trees were acceptably classified according to their nutritional status, which involves a more efficient use of fertilizers compared to the equal distribution of all the trees.

These results encourage the use of on-board multispectral cameras to monitor the nutritional status of trees and to establish a more efficient fertilization strategy where inputs are applied according to individual status, with the consequent reduction in losses of fertilizers, such as nitrogen, either to the atmosphere, soil, and/or water, generally derived from local overdose.

This strategy would be aligned with the Common Agricultural Policy (CAP) reform in the European Union, which has set as a remarkable aim the reduction in nutrient losses of at least 50% by 2030, which is expected to lead to a reduction in fertilizer use of at least 20%.

Author Contributions: Conceptualization, P.B. and L.L.; methodology, V.L., J.V., P.B. and L.L.; data acquisition and analysis, V.L., P.B. and L.L.; software and formal analysis of the data, P.B., L.L. and N.H.-S.; investigation, P.B., N.H.-S. and L.L.; resources, V.L. and P.B.; supervision, P.B., N.H.-S. and L.L.; writing—original draft, P.B., N.H.-S. and L.L.; writing—review and editing, P.B., N.H.-S. and L.L. All authors have read and agreed to the published version of the manuscript.

Funding: This research received no external funding.

Data Availability Statement: Not applicable.

Acknowledgments: We gratefully acknowledge Jean-Michel Roger from INRAE (Montpellier, France) for his support in spectral analyses.

Conflicts of Interest: The authors declare no conflict of interest.

References

1. Belkhodja, R.; Morales, F.; Sanz, M.; Abadía, A.; Abadía, J. Iron deficiency in peach trees: Effects on leaf chlorophyll and nutrient concentrations in flowers and leaves. *Plant Soil* **1998**, *203*, 257–268. [CrossRef]
2. Lafuente, M.V.; Lleó, L.; Roger, J.M.; Barreiro, P. SPAD and hyperspectral images for sensing chlorosis affection in peach trees. In Proceedings of the European Conference on Agricultural Engineering AgEng2018, Wageningen, The Netherlands, 8–12 July 2018.
3. Lafuente, M.V.; Barreiro, P.; Lleó, L.; Val, J. Prognosis of leaf chlorosis in Catherina peaches based on the mineral composition of flowers. In Proceedings of the European Conference on Agricultural Engineering AgEng2018, Wageningen, The Netherlands, 8–12 July 2018.
4. Barreiro, P.; Veganzones, A.; Lafuente, V.; Lleó, L.; Hansen, M.; Val, L. A procedure for monitoring the phenological status of peach flowers with artificial vision. In Proceedings of the XX CIGR World Congress 2022, Kyoto, Japan, 5–10 December 2022.
5. Igartua Arregui, E.; Grasa, R.; Sanz Encinas, M.; Abadía Bayona, A.; Abadía Bayona, J. Prognosis of iron chlorosis from the mineral composition of flowers in peach. *J. Hortic. Sci. Biotechnol.* **2000**, *75*, 111–118. [CrossRef]
6. Ustin, S.L.; Jacquemoud, S. How the Optical Properties of Leaves Modify the Absorption and Scattering of Energy and Enhance Leaf Functionality. In *Remote Sensing of Plant Biodiversity*; Cavender-Bares, J., Gamon, J.A., Townsend, P.A., Eds.; Springer: Cham, Switzerland, 2020; pp. 349–384.
7. Zahir, S.A.D.M.; Jamlos, M.F.; Omar, A.F.; Muncan, J.; Tsenkova, R. Review—Plant nutritional status analysis employing the visible and near-infrared spectroscopy spectral sensor. *Spectrochim. Acta-Part A Mol. Biomol. Spectrosc.* **2024**, *304*, 123273. [CrossRef]
8. Fernández, V.; Eichert, T.; Río, V.; López-Casado, G.; Heredia-Guerrero, J.; Abadía, A.; Heredia, A.; Abadía, J. Leaf structural changes associated with iron deficiency chlorosis in field-grown pear and peach: Physiological implications. *Plant Soil* **2008**, *311*, 161–172. [CrossRef]
9. Ling, Q.; Huang, W.; Jarvis, P. Use of a SPAD-502 meter to measure leaf chlorophyll concentration in Arabidopsis thaliana. *Photosynth. Res.* **2011**, *107*, 209–214. [CrossRef] [PubMed]
10. Galanti, R.; Cho, A.; Ahmad, A.; Mollinedo, J. Use of a Chlorophyll Meter for Nondestructive and Rapid Estimation of Leaf Tissue Nitrogen in Macadamia. *HortTechnology* **2019**, *29*, 308–313. [CrossRef]
11. Mishra, P.; Asaari, M.S.M.; Herrero-Langreo, A.; Lohumi, S.; Diezma, B.; Scheunders, P. Close range hyperspectral imaging of plants: A review. *Biosyst. Eng.* **2017**, *164*, 49–67. [CrossRef]
12. Guo, Y.; Chen, S.; Li, X.; Cunha, M.; Jayavelu, S.; Cammarano, D.; Fu, Y. Machine Learning-Based Approaches for Predicting SPAD Values of Maize Using Multi-Spectral Images. *Remote Sens.* **2022**, *14*, 1337. [CrossRef]
13. Huang, S.; Tang, L.; Hupy, J.; Wang, Y.; Guofan, S. A commentary review on the use of normalized difference vegetation index (NDVI) in the era of popular remote sensing. *J. For. Res.* **2021**, *32*, 1–6. [CrossRef]
14. Lin, K.H.; Huang, M.Y.; Weng, J.H.; Kao, S.C. Photosynthetic activity of red and green leaf sectors in Coleus blumei plants as sensed by chlorophyll fluorescence. *Photosynthetica* **2019**, *57*, 659–667. [CrossRef]
15. Daughtry, C.S.T.; Walthall, C.L.; Kim, M.S.; Brown de Colstoun, E.; McMurtrey, J.E. Estimating Corn Leaf Chlorophyll Concentration from Leaf and Canopy Reflectance. *Remote Sens. Environ.* **2000**, *74*, 229–239. [CrossRef]
16. Grant, L. Diffuse and specular characteristics of leaf reflectance. *Remote Sens. Environ.* **1987**, *22*, 309–322. [CrossRef]
17. Dedeoglu, M. Estimation of critical nitrogen contents in peach orchards using visible-near infrared spectral mixture analysis. *J. Near Infrared Spectrosc.* **2020**, *28*, 315–327. [CrossRef]
18. Abenina, M.I.A.; Maja, J.M.; Cutulle, M.; Melgar, J.C.; Liu, H. Prediction of Potassium in Peach Leaves Using Hyperspectral Imaging and Multivariate Analysis. *AgriEngineering* **2022**, *4*, 400–413. [CrossRef]